J Appl Physiol 113: 328–339, 2012.
First published May 17, 2012; doi:10.1152/japplphysiol.00320.2012.

HIGHLIGHTED TOPIC | *Imaging Lung Physiology*

Imaging lung perfusion

Susan R. Hopkins,[1] Mark O. Wielpütz,[2] and Hans-Ulrich Kauczor[2]

[1]*Departments of Medicine and Radiology, Pulmonary Imaging Laboratory University of California San Diego, La Jolla, California; and* [2]*University Hospital Heidelberg, Heidelberg Thorax Imaging Platform (HTIP), Translational Lung Research Center Heidelberg (TLRC-H), Member of the German Center for Lung Research, Heidelberg, Germany*

Submitted 13 March 2012; accepted in final form 14 May 2012

Hopkins SR, Wielpütz MO, Kauczor HU. Imaging lung perfusion. *J Appl Physiol* 113: 328–339, 2012. First published May 17, 2012; doi:10.1152/japplphysiol.00320.2012.—From the first measurements of the distribution of pulmonary blood flow using radioactive tracers by West and colleagues (*J Clin Invest* 40: 1–12, 1961) allowing gravitational differences in pulmonary blood flow to be described, the imaging of pulmonary blood flow has made considerable progress. The researcher employing modern imaging techniques now has the choice of several techniques, including magnetic resonance imaging (MRI), computerized tomography (CT), positron emission tomography (PET), and single photon emission computed tomography (SPECT). These techniques differ in several important ways: the resolution of the measurement, the type of contrast or tag used to image flow, and the amount of ionizing radiation associated with each measurement. In addition, the techniques vary in what is actually measured, whether it is capillary perfusion such as with PET and SPECT, or larger vessel information in addition to capillary perfusion such as with MRI and CT. Combined, these issues affect quantification and interpretation of data as well as the type of experiments possible using different techniques. The goal of this review is to give an overview of the techniques most commonly in use for physiological experiments along with the issues unique to each technique.

magnetic resonance imaging; computerized tomography; positron emission tomography; single photon emission computed tomography; blood flow; pulmonary

QUANTITATIVE IMAGING OF REGIONAL pulmonary perfusion is a field that continues to develop rapidly, and there are a number of techniques available using imaging modalities such as magnetic resonance imaging (MRI), computerized tomography (CT), and radioisotopes. A multitude of issues must be considered when using imaging to measure regional pulmonary blood flow, including what is actually being measured—does the technique provide a measure of true perfusion, and how is the measurement expressed, per unit volume, per alveolar, per gram of water or relative to mean perfusion? Some of the most common methods of measuring regional pulmonary blood flow and regional perfusion are discussed below along with the advantages and limitations of each from the perspective of conducting physiological studies.

ISSUES WITH MEASURING PERFUSION IN THE LUNG COMMON TO ALL IMAGING TECHNIQUES

Acquiring Data

The distribution of pulmonary perfusion is influenced by multiple factors including, among others, respiratory motion, regional lung mechanics, gravity, and inspired gas mixtures. Thus when reading and interpreting the imaging literature it is important to consider the measurement conditions and other issues. For example, respiratory motion during breathing induces pressure and subsequently volume changes within the chest, which in turn affect blood flow and regional perfusion. As the pulmonary circulation is a low pressure system, it is potentially affected by pressure changes induced by breathing, lung volume, and breath holding (24).

Pulmonary blood flow is reported to be more than double in expiration compared with inspiration (287 vs. 129 ml·min^{-1}·100 ml^{-1}, respectively) (18). This effect is also be observed when scanning was performed in prone posture, expiration vs. inspiration (271 vs. 99 ml·min^{-1}·100 ml^{-1}, respectively) (18). However, it is incorrect to think of this as largely a physiological effect on blood flow. Rather, this is because in inspiration a voxel contains more air and thus the signal observed by external imaging devices is reduced and consequently so is the perfusion measured per unit volume (Fig. 1). When blood flow is expressed per gram lung this apparent effect can largely be circumvented, allowing comparisons between different states of lung inflation (38).

The influence of gravity on the distribution of pulmonary blood flow is well described (7, 15, 45, 49, 58). An apical to basal gradient is well known from chest radiography performed in erect posture and posterior-anterior projection. In cross-

Address for reprint requests and other correspondence: S. R. Hopkins, Professor of Medicine and Radiology, Division of Physiology 0623A, Univ. of California, San Diego, 9500 Gilman Dr., La Jolla, CA 92093 (e-mail: shopkins@ucsd.edu).

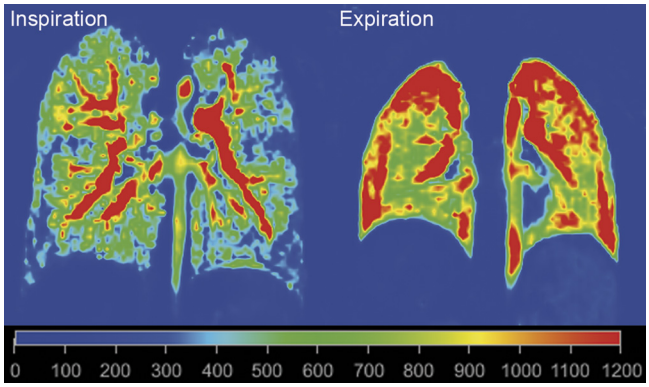

Fig. 1. When measuring lung perfusion, especially with repeated examinations, the lung volume has to be taken into account. *Left*: contrast-enhanced MRI perfusion study of a healthy volunteer in full inspiratory breath hold, i.e., total lung capacity. Large vessels can easily be identified. Mean pulmonary blood volume (PBV) as computed by a dedicated software tool (PulmoMR, Fraunhofer MEVIS, Bremen) is ~28.1 ml·100 ml^{-1} of lung. In expiration, i.e., residual volume, mean PBV rises to ~62.9 ml·100 ml^{-1}. Scale equals ml·100 ml^{-1}. Courtesy of J. Ley-Zaporozhan, Toronto, and P. Kohlmann, Bremen.

sectional imaging using CT and MRI in a supine posture, an obvious anterior-posterior gradient can be observed (18, 21), which is reversed into a posterior-anterior gradient in prone (18, 21). In part these observed gradients are a result of gravitationally induced tissue distortion and alterations in regional density (38, 75), such that the gravitationally dependent lung will contain more lung tissue (blood vessels) termed the "Slinky effect" (38). Some authors have suggested that the blood flow distribution in prone posture is more uniform than in supine (90), although this is not a consistent finding (80). In upright posture the gravitational effect on pulmonary blood flow has been shown to be most pronounced at total lung capacity (TLC), reduced at residual volume (RV) (41). However, more recent work in healthy supine subjects has shown that the influence of gravity on the distribution of blood flow is remarkably similar, irrespective of lung volume, except in the most nondependent portion of the lung in which it is reduced at TLC compared with other lung volumes (35).

Many techniques that image pulmonary blood flow require the subject to hold his/her breath during acquisition, and this has the potential to alter arterial blood gas values (87). Although potentially important (91), the typical duration of breath holding is not long enough during imaging to have significant effects. For example, hypoxic pulmonary vasoconstriction is maximal by 20 min (87), and this relatively long response time combined with the small changes induced in arterial P_{O_2} during a breath hold of ~30 s means that any affects are likely to be insignificant. However, the half-time for the maximal pulmonary vascular response to CO_2 is ~90 s (91), and consequently small changes in regional perfusion resulting from the increased concentrations of CO_2 during breath hold scanning are possible.

Quantification

Data sets derived from regional measurements of pulmonary perfusion can be extremely large, and a significant challenge is determining how best to express quantitative regional data to answer physiological questions. Mean perfusion can be measured by simply measuring cardiac output—imaging is not required. Thus regional (spatial) data have attracted the most attention from physiologists. Spatial gradients can be described as linear regressions of data against spatial location, for example, as height from dependent lung in the case of questions related to the influence of gravity (35, 38, 80). However, this distills large amounts of information down to a dozen or so data points. Several metrics have been used to describe regional heterogeneity, and a discussion of data analysis techniques for regional data can be found in the review by Glenny (28). For example, the relative dispersion (standard deviation/mean, also known as the coefficient of variation) globally quantifies the extent of spatial heterogeneity, but reduces all heterogeneity to a single number without regard to the spatial location (31, 37). Fractal analysis (28) describes the extent to which the pattern of blood flow is self similar, i.e., the extent to which blood flow in one region is correlated with flow in adjacent regions of the lung. To be fractal in nature, this relationship must hold for all regions, regardless of size or location. The fractal dimension (Ds) is calculated as the slope of the relationship of the plot of log piece (voxel) size and the log relative dispersion and is described in detail in (4). This slope calculation starts with the largest piece sizes of the image, which has the lowest relative dispersion. As the piece size become smaller (i.e., the resolution of the observation is finer) the standard deviation (and thus the relative dispersion) becomes larger, and least squares regression is used to calculate the slope. However, the points at the largest piece size may deviate from this linear relationship and thus are excluded.

Another approach, cluster analysis, groups regions of lung into bins or "clusters" that share similar blood flow patterns or responses to a stimulus. The regions are binned without spatial information and then once identified by their response, anatomically located and described. Another metric, spatial correlation, is the correlation coefficient between perfusion measurements for all locations within the lung that is used to generate a plot of correlation coefficient r vs. separation distance. The zero-crossing point (distance of zero correlation) is a measure of the scale of the major components of the heterogeneity within the image (28).

Challenge of Validation

Reliability is the ability of a measurement to give the same value when repeated under the same conditions, and will, in the real world, incorporate any biologic variability present in addition to measurement variability. Reliability of a technique can be established by making a number of repeated measurements both within an imaging session and over a period of days or weeks, and thus is readily determined. Validity, a measure of how well a technique measures what it is designed to measure is often more difficult to establish. Imaging techniques, which rely on intravascular contrast for measurement, may not measure perfusion per se. This is because perfusion is defined as the nutritive delivery of blood to the capillary bed (17), and some techniques may label blood in conduit vessels (i.e., arteries and veins) in addition to that in the capillary circulation. Also because regional information is the most valuable data derived from imaging, the lack of a gold standard that can be used in humans makes direct validation studies more difficult. For example, microsphere measurements cannot be performed in humans, and when used (i.e., in animal

studies) a limitation of the technique is that it will not reflect any effect that regional variations in lung tissue density will have on the measurement of regional perfusion using external imaging such as MRI (38).

The establishment of validity takes multiple steps: first, do the data agree with expected data? Because the volume of a normal human lung in supine posture at functional residual capacity is ~4 liters (~3 liters air and 1 liter tissue) and resting cardiac output is ~5–6 l/min, mean regional blood flow is expected to approximate 1.3–1.5 $ml \cdot min^{-1} \cdot ml^{-1}$, or taking a value of 1 kg for the weight of the whole lung ~5 - 6 $ml \cdot min^{-1} \cdot g^{-1}$. Second, does the summed blood flow measured in the lung agree with the measurement of cardiac output under identical conditions? Because different spatial distributions (i.e., different blood flow distributed to different anatomic locations) can give the same total flow, poor agreement is clearly a sign that the technique is not valid, but good agreement does not ensure validity. Third, are similar numbers obtained when the technique is cross validated against other techniques offering spatial information? This is difficult because the ideal technique should not be subject to significant measurement error itself. It is important to recognize that many of the techniques discussed below have not been fully validated, but are based on established physical principles and are likely reasonably valid, especially given the limited alternatives in humans. In particular, MRI techniques, which do not expose subjects to risks from ionizing radiation, have been widely used in healthy and diseased humans to study different physiological and pathophysiological conditions, but validation by often far more invasive gold standard is difficult to achieve.

Potential Error Sources

A measure of the amount of detail contained in an image for all imaging techniques is resolution—that is the minimal distance of two separate points (or volume elements called voxels) at which the technique can still identify them as such. An issue that affects the visualization and quantification of pulmonary perfusion is called partial volume effect, which is a consequence of the resolution of the acquisition. Partial volume means that the measurement of any one voxel is not independent of surrounding voxels—some signal is lost into adjacent voxels and some is gained as spillover from adjacent voxels, leading to averaging of information as consequence of a spatial resolution that is greater than the voxel size to be imaged. An edge effect occurs when the voxel of interest is near the edge of the lung and results in apparent loss of signal into regions outside the lung.

As already mentioned above, respiratory and cardiac motion will disturb the exact spatial coding of a signal to be imaged. This can be either obviated by fast imaging techniques within a single breath hold and cardiac diastole or by parallel registration of respiratory motion and an electrocardiogram during imaging. The latter can either be used to produce snapshot images at predefined time points of the respiratory or cardiac cycle (prospective gating). Or a continuous data set is acquired over a longer time period, which will retrospectively be separated into different phases (retrospective gating). Some techniques also allow for computing the different phases from the data set itself without external recording of the respiratory or cardiac cycle (intrinsic retrospective gating). The technique of gating is especially important when long acquisition times become necessary to produce sufficient signal.

Another issue is the integration of separate data sets of the same object, for example structural information from CT and functional information from single photon emission computed tomography (SPECT), to create superimposed images. This fusion of information requires that only voxels of the same coordinates are superimposed. Either both techniques are combined into a single scanner system (e.g., SPECT/CT), or complicated postprocessing is needed to identify and fuse identical structures in both imaging sequences (called registration). Moreover, registration of two techniques may not easily be transferred to a third imaging method.

All techniques differ substantially in the balance between temporal and spatial resolution, and the amount of energy externally applied to the subject to record signal. These issues are discussed in the following text and also summarized in Table 1.

TECHNIQUES AVAILABLE FOR MEASURING PERFUSION

MRI

MRI has the potential for comprehensive structural and functional imaging of tissue without risk from ionizing radiation. However, proton-MRI of the lung is extremely challenging due to three main reasons: first, the low amount of tissue only contains a small number of protons, which is directly related to low signal. Second, the multiple air-fluid interfaces in the lung cause substantial susceptibility artifacts that result in a rapid decay of signal. Third, respiratory, vascular and cardiac motion (57) affect image registration and intrinsic resolution. Standard MR scanners with a field strength of 1.5 T and full parallel imaging capabilities are generally thought to optimize MRI of the lung (11, 82). Although a higher field strength, i.e., 3.0 T, will theoretically increase the signal-to-noise ratio, the susceptibility artifacts are more pronounced and lead to an even faster signal decay.

Contrast enhanced MRI. When performing MRI studies of lung perfusion with contrast media, sequences with an emphasis on either high spatial or high temporal resolution are utilized. The first has been termed MR angiography (MRA), the latter MR perfusion imaging. First, a T1-weighted sequence is acquired before the intravenous injection of a Gadolinium-based contrast using a contrast power injector. The highest spatial resolution for MRA is currently achieved with T1-weighted 3D gradient echo acquisitions (12, 60). The whole thorax can be covered within a single breath hold of less than 20 s and a voxel size of as low as $1.0 \times 0.7 \times 1.5$ mm. On the basis of such data sets multiplanar reconstructions (MPR) can be computed in arbitrary angulations and 3D visualization can be achieved just as for multidetector CT data sets. When moving from a single phase acquisition to a multiphasic acquisition the different vascular territories, pulmonary arterial, pulmonary parenchyma, and pulmonary venous as well as systemic arterial can be visualized separately. By subtracting the nonenhanced sequences acquired upfront an even better visualization of the different intrathoracic vascular territories is achieved. This information is important to diagnose anomalies of the thoracic vasculature and their functional impact, e.g.,

Table 1. *A quick guide to the various imaging techniques*

Technique	Pros	Cons
MRI		
Contrast Enhanced	-high spatial resolution, largely measures capillary perfusion if thresholds applied. -high temporal resolution in order of 1 s -good SNR -availability -somewhat repeatable (need time to clear tracer material) -no radiation	-potential allergic reactions to contrast -limited validation data in the lung, although those available show high validity -quantification limited by non-linearity between contrast concentration and signal -moderately invasive (iv injection) -no correction for tissue density as typically implemented
Phasecontrast	-high sub-second temporal resolution -availability -quantitative -no contrast injection -somewhat repeatable - no radiation	-limited spatial information, measures blood flow in large vessels only single slices -limited validation data -no correction for tissue density as typically implemented
ASL	-quantitative -highly reliable -largely measures capillary perfusion if thresholds applied - can be corrected for tissue distribution -repeated measures possible -no radiation -noninvasive -no contrast injection	-technically difficult -limited sampling of lung (single slice as currently implemented) -low SNR -limited availability - moderate spatial resolution -relatively expensive -limited validation data in the lung, although those available show high validity
Nuclear Medicine		
SPECT	-widely available -relatively inexpensive -measures capillary perfusion (no conduit vessel contribution) -semi-quantitative: attenuation corrections required -perfusion measurements are expressed relative to mean perfusion	-limited spatial resolution -long acquisition time -moderately invasive (iv injection) -limited repeatability because of radiation and time to clear tracer material -no correction for tissue density as typical implemented -modest radiation exposure: ~2 mSv/study*
PET	-high spatial resolution -measures capillary perfusion (no conduit vessel contribution) - semi-quantitative: perfusion measurements are expressed relative to mean perfusion	-limited repeatability because of radiation exposure -moderately invasive (iv injection) -no correction for tissue density as typical implemented -limited availability -relatively expensive -limited validity data - moderate radiation exposure: ~ 5–7 mSv/study*
CT	-maximum spatial resolution -excellent detail of the vasculature -visualization of capillary blood content (DECT)	-limited repeatability - modest radiation exposure: 1–5 mSv*, higher for perfusion studies -limited temporal resolution with respect to radiation -DECT non-quantitative, visual evaluation only -potential allergic reactions to iv contrast

* As typically implemented. Detailed review of exposure data in (10, 22, 50, 62).

pulmonary artery atresia, pulmonary arteriovenous malformations, or anomalous pulmonary venous return.

MR perfusion imaging is a straightforward and easy-to-implement technique. Its basic principle is a dynamic acquisition before, during, and after an intravenous bolus injection of contrast using a power injector. Very short acquisition times for complete 3D datasets of the thorax of less than 1.5 s by combining parallel imaging and echo sharing allow for the continuous imaging during the passage of the contrast bolus, so called four-dimensional (4D or 3D + t), or dynamic first-pass perfusion MRI. This high temporal resolution acquisition is required to visualize perfusion during the peak enhancement of the normal lung parenchyma as well as lung areas with delayed pulmonary arterial perfusion and systemic, bronchoarterial perfusion (23, 26, 53) in different disease states. As for MRA, subtracted data sets are provided. Spatial resolution of these data sets is ~3.0 × 1.5 × 4.0 mm, allowing for the analysis of pulmonary perfusion down to a subsegmental level. The technique is widely used clinically including the precise anatomic allocation of perfusion defects to individual lobes and segments, such as in acute and chronic pulmonary embolism (25, 54), in small airway diseases, chronic obstructive pulmonary disease (COPD) (5, 64, 92), and cystic fibrosis (20) (Fig. 2). The reversibility of perfusion defects after a therapeutic intervention serves as an indicator for response to therapy and potentially differentiates between regions of reversible and irreversible disease. Quantitative measurements of pulmonary perfusion have been established using different techniques. The most robust is the measurement of the mean transit time (MTT) derived from time-resolved contrast-enhanced 3D + t perfusion data sets, which can be complemented by the calculation of pulmonary blood flow (PBF) and blood volume (PBV), all based on the indicator dilution theory. These parameters have been used to evaluate patients with COPD (70)

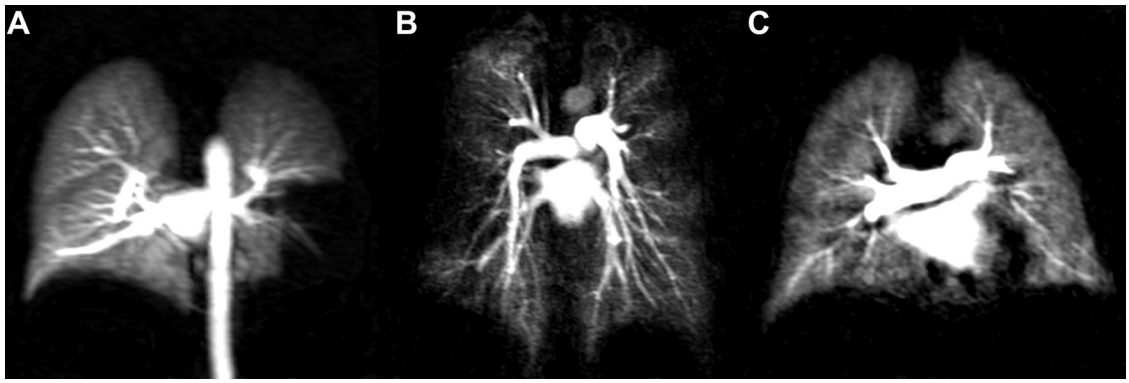

Fig. 2. *A*: occlusion of pulmonary vessels will lead to sharply delineated perfusion defects as in this case of acute pulmonary embolism of the left inferior lobe in the pulmonary perfusion MRI [maximum intensity projection (MIP) image]. Perfusion of the right lung remains unimpeded. *B*: in contrast, cystic fibrosis with its extensive mucus obstruction of airways goes along with large hypoperfused areas in both lungs (MIP). *C*: chronic obstructive pulmonary disease COPD with concomitant emphysema shows a generally lower degree of contrast enhancement as well as diffuse patchy perfusion defects predominantly of the superior lobes (MIP).

and pulmonary arterial hypertension (55, 70) compared with healthy subjects. Of the aforesaid parameters, MTT correlated best ($r = 0.56$) with pulmonary arterial pressure measured invasively in pulmonary arterial hypertension patients (55). The signal measured with these techniques will encompass smaller arteries as well as the capillaries as current software-based evaluation tools will cut out the pulmonary trunk and larger arteries.

Validation of quantification of PBF with dynamic contrast-enhanced MRI is still challenging. One main reason is the nonlinear dependence of signal intensity (SI) from contrast agent (CA) concentration (83). First-pass perfusion MRI has been compared with $H_2{}^{15}O$ positron emission tomography (PET) imaging (see below) in a porcine model. Calculations of hemodynamic parameters were based on a one-compartment model (MR) and a two-compartment model (PET) (69). MR flow values yielded a significant correlation ($P < 0.001$) in dorsal regions where signal-to-noise ratio (SNR) was sufficient. After correction for nonlinearity the agreement for PBF showed mean values for PET of 59 ml·min^{-1}·100 ml^{-1} lung tissue, and 80 ml·min^{-1}·100 ml^{-1} for MRI (69). The reasons that there is not a better agreement between the two measures is threefold. First, the PET "perfusion" signal is sensitive only to capillary flow, whereas contrast-enhanced MRI has the larger vessel signal incorporated. Second, the spatial coverage and the size of the observed pulmonary regions are different. Third, PET was performed during continuous ventilation, whereas MRI was performed in an expiratory breath hold (61). At the same time two different MR-based measurements, dynamic contrast-enhanced perfusion and phase-contrast MR (see below), provide consistent measures of regional pulmonary blood flow ($r^2 = 0.71$) (99). Dynamic contrast-enhanced MRI has also been validated by microspheres for quantitative measurements of myocardial blood flow with correlation coefficients $r > 0.87$ (40).

Phase-contrast MRI. Cardiac motion leads to a pulsatile flow within the pulmonary vasculature. The flow curves can be easily measured by phase-contrast MRI in the main pulmonary arteries. With this technique, the phase of transverse magnetization—not the intensity of longitudinal magnetization—is used for image composition (27). Moving tissue produces a phase shift when two opposing gradient pulses are applied consecutively, which is directly proportional to its velocity. Such images reflect the pulsatile flow within the intrathoracic vasculature and the cardiac chambers. Laminar or turbulent flow profiles can be identified. Furthermore quantification of blood flow is feasible by integrating the phase information over the whole cross-sectional area of the vessel. Anatomically, pulmonary blood perfusion is composed of two separate afferent systems, the pulmonary arteries transporting deoxygenized blood from the right heart and the bronchial arteries serving as a nutritive system for the lung. When measurements are performed in the pulmonary trunk and the aorta, shunt volumes can be quantified. Under physiological conditions in healthy individuals, the flow within the central pulmonary arteries and the systemic circulation (aorta) is almost identical as the quantitative contribution of the bronchial arterial perfusion is about 1% of the cardiac output (61). In chronic inflammatory lung diseases, such as cystic fibrosis, a dilatation of bronchial arteries is frequently observed. A higher flow in the bronchial arteries leads to a shunt volume from the systemic into the pulmonary circulation, which can be assessed by quantitative phase-contrast MRI demonstrating a higher flow in the aorta than in the pulmonary trunk (29, 56, 72, 98).

ASL. Arterial spin labeling (ASL), a technique widely used in the brain and other organ systems to measure blood flow, has also been used to study the pulmonary circulation (8, 9, 32, 33, 36, 38, 81). The ASL method alters the magnetic properties of protons to be used as a tracer. The basic premise of ASL is quite simple: protons are "tagged" or labeled using radiofrequency (RF) pulses to invert the magnetization in a proximal anatomical location and then imaging the distal slice of interest as labeled protons are delivered with blood inflow [for a detailed description see (17)]. Alternating control images are obtained in the slice, which are subtracted from the tagged image to provide a map of protons delivered to the imaging slice. After allowing for several factors (17), including the effect of the time it takes for the tagged protons to be delivered on the measured signal (T1 relaxation), blood flow can be quantified.

For the lung it might seem logical to simply tag blood in the main pulmonary outflow tract and then wait until it is delivered to all of the pulmonary circulation. However, in addition to the already low intrinsic signal in the lung, T1 relaxation effects

are worsened by transit delays (97), which can be quite long in the lung. Thus tagging of blood in central structures such as the heart as with STAR-HASTE type sequences can be problematic and large vessels (discussed below) dominate. Also, pulmonary blood flow is highly pulsatile, and thus the images must be cardiac-gated to avoid significant measurement errors. Finally, rapid image acquisition within a breath hold is essential, otherwise complex image registration algorithms are required.

One ASL technique that has been used to study pulmonary physiology is a flow sensitive alternating inversion recovery with an extra radio frequency pulse (FAIRER) sequence (59). This sequence both tags and images in the same plane, avoiding issues related to transit delays: two ECG-gated images of the selected slice are taken ~5 s apart (Fig. 3). The two images acquired are different in the way the RF pulses are applied: in the control image (also known as a selective inversion) the pulse is applied only to the imaged slice, plus an overlap at either side to ensure a uniform inversion profile. For the tag image the inversion is applied to the whole chest and thus is called a nonselective inversion. In both images after the inversion pulses are applied, a waiting period of ~80% of the cardiac R-R interval (termed TI, inversion delay, typically 600–800 ms) occurs allowing inflow of blood from a complete systolic ejection, after which the image is acquired during diastole. During the delay period, TI (identical for both control and tag images), arterial blood moves into each voxel of the image plane in proportion to the local blood flow. The effect of inversion pulse *in the image slice* is the same in both the tag and control images, but the effects *outside the image slice* are different between the two. In the control image, the tagged blood flows out of the image in the delay, but arterial blood outside the slice was undisturbed by the inversion and enters the slice fully relaxed and produces signal (Fig. 3*A*). However, in the tag image, the inversion pulse was applied to entire torso, and thus all blood entering and leaving the slice is tagged. Because tagged blood is near the point where the longitudinal magnetization passes through zero (null point) when imaged, the blood signal entering the slice in the tag image is very weak (Fig. 3*B*). Subtraction of the tag and control images and correction for heterogeneity in the receive coil used to increase the SNR yields a map (Fig. 3*C*) of the amount of blood delivered to each voxel during the delay TI (13, 33, 36) and contains signal from both large conduit vessels and capillary perfusion (see below). As implemented in several recent publications the intrinsic spatial resolution (voxel size) is ~1.5 × 3 × 15 mm (~70 or 0.07 cm^3) (8, 36, 38, 81), although smoothing in postprocessing may render it lower resolution—up to 1 cm^3.

This technique has been shown to be highly reliable (52) when measures of heterogeneity ($R^2 > 0.9$) are compared across imaging sessions or days apart. Phantom imaging validation studies using FAIRER show that the ASL signal is linear ($R^2 = 0.98$) with flow over the range expected for the lung (39). ASL-FAIRER has the advantage that it can be repeated multiple times, under various physiological conditions without concern for contrast or radiation dose. By combining multiple single slice acquisitions the entire lung can be imaged in ~3 min.

There are several potential sources of error with ASL-FAIRER in the lung, which may affect absolute quantification of regional perfusion. These have been discussed in detail in a recent publication that used an anatomically realistic computer model of the pulmonary circulation (16) to evaluate error. They are as follows: first, as mentioned above, because of scanner limitations, in the control image, the inversion pulse is applied to the image slice with some overlap outside the slice. This is done to create a uniform inversion across the slice, but this also creates a band on either side of the slice, known as an inversion gap. Because ASL-FAIRER depends on the delivery of blood from outside the gap into the image slice, blood that is in the gap was partially inverted and thus the contribution to the signal in the image from fully relaxed protons is reduced, underestimating flow. Large conduit vessels may also affect the measurements in a complicated manner: for example, any portions of the image that are completely full of tagged blood (i.e., saturated) will not fully reflect local perfusion, and contributions such as from in-plane flow from vessels running within a slice may be underestimated. Additionally, any conduit vessels that deliver blood that is destined for capillary bed

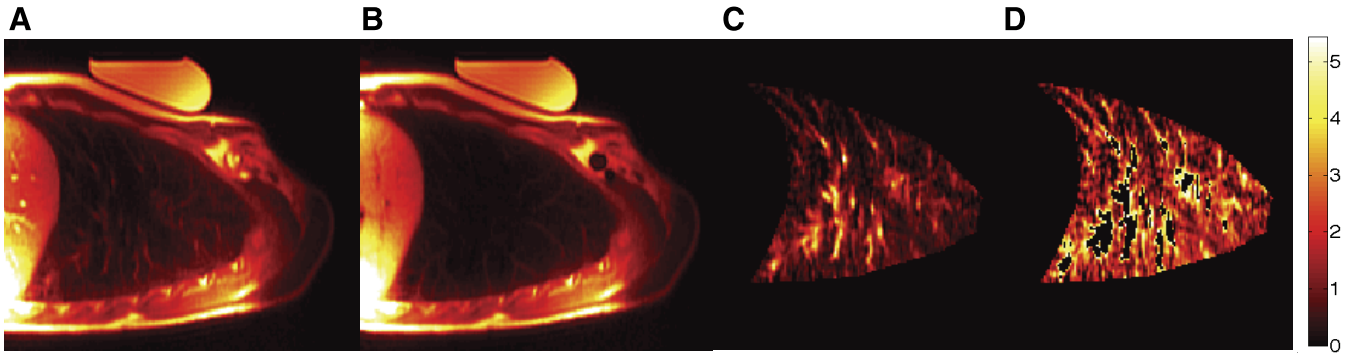

Fig. 3. *A*: ASL-FAIRER MRI measurement of pulmonary blood flow in a single sagittal slice of the right lung in a healthy normal subject. *A* is the control (selective inversion) image. Apex of the lung is to the right of the images, the diaphragm is to the left. Liver is seen as the subdiaphragmatic structure in *A* and *B*. A phantom for absolute quantification is also seen in *A* and *B*. Blood that has not been tagged flows into the image plane and produces signal that is seen as both vascular structures and a blush to the lung periphery. *B* is the tag (nonselective inversion) image where the signal observed is to T1 recovery of longitudinal magnetization after the entire torso has experienced the inversion pulses, which is identical in both *A* and *B*. Subtraction of the tag and control images is seen in *C*, in which stationary signal is subtracted out and gives a map of protons that entered the image plane in *A* during one systolic ejection. Finally, filters are applied to remove contribution from larger conduit vessels (*D*) by eliminating voxels that are more than 35% of the maximum signal intensity, leaving largely perfusion information. Color scale is blood flow in $ml \cdot min^{-1} \cdot ml^{-1}$.

that is not part of the image slice contribute to the overall signal but do not represent perfusion. Finally in the lung, blood in both the pulmonary arteries and veins is tagged and thus contributes to the measured signal. However, with the application of filters in postprocessing (Fig. 3*D*), the contribution of true perfusion to the measured signal is calculated to be ~80% of the total signal (16).

Nuclear Medicine

Some of the earliest measures (41, 102, 103) of regional pulmonary perfusion used radiolabeled gas such as $C^{15}O_2$ or ^{133}xenon. These when inhaled in the case of CO_2, or dissolved in saline and injected intravenously in the case of xenon, permit measurement of time-activity curves made using an external scintillation detector to evaluate portions of the lung with limited spatial resolution. The regional alveolar activity during a breath hold following the intravenous injection of a relatively insoluble gas is a function of regional perfusion. Two-dimensional images of the entire lung were possible with the development of the planar gamma camera, and more recently, radionuclide methods have used a variety of radioactive or radiolabeled compounds to measure pulmonary perfusion in three dimensions.

SPECT. SPECT relies on multiple detection of photons from a gamma-emitting source that is reconstructed into a 3D image (77, 78). To measure pulmonary perfusion the most widely used technique involves the injection of Technetium-99m labeled macroaggregated albumin (^{99m}Tc-MAA) (76–78). These particles act like microspheres and lodge in pulmonary capillaries in proportion to local blood flow (Fig. 4). Thus a significant advantage of SPECT with ^{99m}Tc-MAA is that it is a measure of true perfusion, as the size of the particles (10–150 μm) means that they are distributed to small pulmonary arterioles and capillary beds and are not located in large conduit vessels. Other tracers used to measure pulmonary blood flow include ^{113m}indium-MAA (73, 77), which is used in a similar fashion to ^{99m}Tc-MAA, and ^{81m}krypton (71), which is used as a steady-state intravenous infusion.

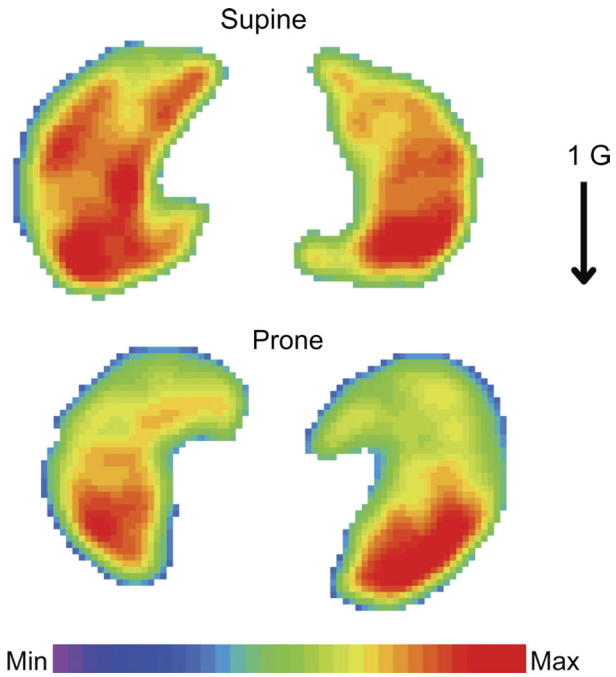

Fig. 4. ^{99m}Tc-MAA SPECT images of pulmonary perfusion in the axial plane of both lungs obtained from a healthy normal volunteer in prone and supine posture. Perfusion is increased in the dependent lung in both postures. In part this is due to gravitationally induced lung tissue deformation inside the thorax. [Figure modified with permission from (74).]

Typical acquisition times for SPECT images are on the order of several minutes and thus the subject must breathe quietly during the acquisition. The resolution of the technique is thus affected by respiratory motion. Respiratory gating can compensate for resulting blurring or smearing of the recovered image but has the disadvantage of further increasing the acquisition time. Physical interaction of the emitted photon with tissue results in scattering and attenuation, which must be corrected for to produce quantitative data. This is because scattering changes both the direction and the energy of the photon in a manner that is dependent on the nature of the tissue, the energy of the photon used, and the distance of travel. Typically transmission tomography is used to obtain data for the attenuation correction (2, 3, 86) and involves the acquisition of an attenuation (density) map using an external radiation source. Phantom studies have demonstrated that attenuation correction gives a reasonable correction. Alternatively, combined SPECT-CT scanners simultaneously acquire a volumetric density profile with identical coordinate systems, and this density map is used in the SPECT attenuation reconstruction (30). The advantage of combined scanners is that, because a CT image is also reconstructed, the functional data from SPECT can be superimposed with the structural CT data without registration.

SPECT is widely available and relatively inexpensive. The specific disadvantages of SPECT to measure regional pulmonary perfusion include difficulty in correcting for the effects of lung volume or tissue density gradients unless a CT image of density is acquired. Also, as typically implemented SPECT measures of perfusion are semiquantified relative to the overall mean perfusion (assigned value of 1.0) and thus is not sensitive to changes that result in overall changes. Finally, although the radiation dose with a single acquisition is relatively modest (~2 mSv), this can rise significantly when physiological studies are planned, requiring repeated measurement.

PET. PET differs from SPECT in that the radiotracer used decays and emits positrons (66, 84). These positrons on collision with electrons emit two photons (called annihilation photons) of equal energy traveling in exactly opposite directions, which are then detected by rings of externally arranged crystals. There is only a few millimeters of distance traveled by the positron before the collision, and by measuring the coincident annihilations a 3D map of the radioisotope concentration can be constructed. Common radioisotopes used in imaging pulmonary blood flow are $^{13}N_2$ and $H_2{}^{15}O$.

$^{13}N_2$-PET imaging of pulmonary perfusion exploits the low solubility of nitrogen ($\lambda \sim 0.02$). During a breath hold a bolus of $^{13}N_2$ dissolved in saline is injected intravenously and is evolved into the alveolar space during the first pass of the tracer through the lung. Thus the local concentration reflects local perfusion (65, 67, 84, 100, 101). Because the $^{13}N_2$ is confined to alveoli that have been perfused by pulmonary capillaries the regional concentrations of $^{13}N_2$ do not reflect measures of flow in conduit vessels but rather perfusion. Similar to SPECT, transmission scans must be obtained to correct the emission scans for attenuation and scatter. An

advantage of $^{13}N_2$-PET is that radiation exposure is reduced compared with ^{99m}Tc-MAA-SPECT, both because of a shorter physical half-life and more rapid elimination via exhaled air.

The use of $H_2{}^{15}O$ to measure perfusion differs from $^{13}N_2$ in that the tracer is infused intravenously at a constant rate during a breath hold and a time activity curve is obtained (63). A second scan some minutes later is used to calculate the $H_2{}^{15}O$ tissue-blood partition coefficient. The input function is measured by constant rate sampling of pulmonary arterial blood (invasive) or by measuring the activity in a region of interest in the right heart using PET, and the regional blood flow is calculated by using the Kety model describing tracer kinetics (46, 47).

For both of these PET techniques, partial volume effects can affect quantitative accuracy, but resolution is relatively good compared with SPECT and ASL-MRI. PET acquisitions of perfusion data are typically quick (within a breath hold), limiting the time required to conduct studies. However, the entire thorax is not contained in the field of view (~10–20 cm), and thus the whole lung is not imaged. As typically implemented PET reports pulmonary perfusion per unit volume, without correction for lung tissue gradients, although it is possible to correct for lung density. PET tracers involve radiation, which precludes multiple studies on the same subjects under differing conditions, and although becoming more widely available, access to PET for research is limited compared with MRI, CT, or SPECT. $H_2{}^{15}O$-PET measures of regional perfusion have been validated against PET measures of perfusion with ^{68}Ga-macroaggregates of albumin (63, 89) with good agreement.

CT

Historically, plain film x-ray was employed clinically to estimate lung blood flow by differences in caliber of the pulmonary vasculature and regional transparency of the lung areas. For example, acute pulmonary embolism (PE) results in localized hypoperfusion due to vascular occlusion and a subsequent redistribution of blood flow. The pulmonary artery proximal to the embolic obstruction will dilate (prestenotic dilatation), whereas the caliber of the distal pulmonary arterial branches will decrease. Due to the subsequent localized hypoperfusion in the distal lung the affected area can be delineated as an area of low attenuation compared with the nonaffected lung, which might even exhibit an increase in attenuation due to compensatory hyperperfusion. In the era of multidetector computed tomography (MDCT) an estimation of lung perfusion is still achieved by assessing local differences in lung density, i.e., attenuation values measured in Hounsfield units (HU). In healthy individuals, a ventrodorsal increase may be observed when scanning in supine posture. Differences in and redistribution of pulmonary blood flow, e.g., because of the reflex of hypoxic vasoconstriction (Euler-Liljestrand effect) (44) is seen as a patchy pattern of different lung attenuation values on inspiratory CT scans, termed "mosaic perfusion." Minimum intensity projections (MinIP) are used to enhance the depiction of mosaic perfusion patterns (85). For this reconstruction technique, images are created by projecting the minimum attenuation value within a stack of images, e.g., 5 mm, onto a single plane voxel.

With the introduction of contrast enhanced computed tomographic angiography (CTA) the direct visualization of the intrathoracic vasculature became feasible (6). Contrast media for CTA contains a defined amount of complexed iodine, used because of its high atomic number and attenuation properties, and is injected intravenously usually by a power injector. Different iodine concentrations, injection rates (ml/s), and injection time (s) are used to define a contrast bolus usually followed by saline chaser. At first pass through the lung different phases can be distinguished: the pulmonary arterial, pulmonary venous, and systemic arterial phase overlap, but depending on the bolus formation a peak enhancement in each vascular segment can be observed. To determine the timing of these phases in subjects of differing age and cardiovascular health, usually a test bolus of a minimum amount of contrast at the predetermined injection rate is tracked with repeated scans at high temporal resolution, and the time point of maximum enhancement in the pulmonary trunk or ascending aorta is measured, giving the circulation time from injection to the target vessel. Another option in modern MDCT is to start with full-dose contrast material injection while monitoring the enhancement within the target vasculature and triggering the volumetric acquisition of the whole thorax when a predefined threshold attenuation value is reached.

Depending on the timing, images with isotropic submillimeter resolution of the pulmonary vascular tree can be achieved. Dilated bronchial arteries may also be detected, which appear as contrast-filled mainly in the systemic-arterial phase (43). Because these data sets show equal resolution in all three dimensions, multiplanar reconstructions (MPR) can be computed in arbitrary angulations and allow for 3D visualization. Maximum intensity projections (MIP), for which the voxels of the maximum attenuation value of a predefined volume are projected onto one plane are helpful to delineate the pulmonary vascular tree down to the subsegmental level. However, it has to be kept in mind that this represents visualization of the vascular tree, but not capillary perfusion.

To quantify pulmonary blood flow by MDCT, continuous or repetitive time-resolved (4D) ECG-gated scans of a lung volume during contrast bolus injection are necessary, however, at the expense of additional radiation exposure. Initially limited to small lung volumes, the latest generation of scanners may cover the whole lung for such studies. Time-attenuation curves of the lung vasculature and parenchyma can be created, measuring regional pulmonary blood flow and mean transit time (1, 19). Pulmonary microvascular blood flow can be derived by subtracting the contribution of large arteries from the signal (104).

A more direct approach to image pulmonary blood distribution by CT, which can be combined with CTA, is dual-energy CT (DECT). High-end scanners provide the opportunity to examine subjects simultaneously emitting two separate x-ray spectra. Technically, this has been realized by fast alternations of x-ray tube voltage ("fast kV switching") or by mounting two separate x-ray tubes and detector arrays onto one CT gantry ["dual source CT" (DSCT)] (48). Because x-ray absorption is dependent on the nuclear number, a rough material decomposition into water, iodine, and calcium can be computed (42). Thus DECT has the potential for the visualization of the distribution of iodinated contrast within the lung parenchyma after intravenous administration, visualizing regional perfused

blood volume—not lung perfusion (96). This can be depicted by an overlay of color-coded maps, showing a typical supine gravity-dependent ventrodorsal gradient of lung blood flow in healthy individuals. In cases of acute pulmonary embolism for example, wedgelike defects occur (79, 94); in chronic obstructive pulmonary disease (COPD) diffuse patchy hypoperfused areas are present (105). Several consecutive scans of the lung volume or continuous scans solely of a single axial slice may also be combined to snapshot images of a time course of lung perfusion to detect areas of delayed or broncho-arterial perfusion (see also section on contrast enhanced MRI). A typical DECT scan of the thorax will expose the human subject to radiation in the order of 5 mSv, which limits its applicability for physiological studies, especially with respect to repeatability.

However, generated color maps allow only a semiquantitative evaluation of pulmonary blood flow. The visualization of pulmonary blood flow by DECT has been cross validated with ^{99m}Tc-MAA perfusion scintigraphy and SPECT/CT, both showing a good agreement in the detection of perfusion defects with a κ-value of 0.70 as well as a sensitivity between 75 and 100% and a specificity ranging from 76 to 100% (68, 93, 94). Quantification of pulmonary perfusion from DECT beyond the assessment of perfusion defects is still experimental and has not been validated. However, measurements of lung perfusion by MDCT have the potential to cross validate measurements of perfused blood volume by DECT and to translate DECT into a measure for pulmonary perfusion. MDCT and DECT provide a unique combination of structural and functional information at the highest spatial resolution available in radiological imaging (34).

FUTURE DIRECTIONS

The techniques for imaging of regional pulmonary perfusion are developing rapidly and many refinements and changes are expected in the future. With a move to using these techniques in physiological research it is anticipated that reliability and validity will continue to improve. In addition, because of the largely noninvasive nature of imaging it opens the door to studies in humans that would have previously required an animal model. Human studies are of critical importance because there are marked species differences in the extent of hypoxic pulmonary vasoconstriction (51). For example, dogs have very little hypoxic pulmonary vasoconstriction, whereas pigs are the opposite (51). These differences have important clinical implications. In acute lung injury (ALI) it has been shown that regional pulmonary perfusion is reduced in areas of edematous lung as a result of hypoxic pulmonary vasoconstriction (14) in animal models. However, in humans with ALI and cardiogenic pulmonary edema, it has been demonstrated using PET that regional blood flow is not altered in areas of edema suggesting vascular dysfunction (88). Additionally imaging techniques may enable types of measurements that have not been previously possible. One such measurement is of the temporal fluctuations in pulmonary blood flow. The use of ASL-FAIRER is now possible to make repeated measurements of a single slice of lung at a temporal resolution of ~8 s. This allows not only the spatial but also the temporal fluctuations in blood flow to be measured, opening up a whole new metric for evaluating the lung in health and disease. For example, such 4D measurements will open a broad investigation of the effects of respiratory motion and breathing maneuvers as well as cardiac and vascular pulsation onto pulmonary perfusion.

GRANTS

This work was supported by National Heart, Lung, and Blood Institute Grant R01 HL081171.

DISCLOSURES

No conflicts of interest, financial or otherwise, are declared by the authors.

AUTHOR CONTRIBUTIONS

Author contributions: S.R.H., M.O.W., and H.-U.K. conception and design of research; S.R.H., M.O.W., and H.-U.K. interpreted results of experiments; S.R.H., M.O.W., and H.-U.K. prepared figures; S.R.H., M.O.W., and H.-U.K. drafted manuscript; S.R.H., M.O.W., and H.-U.K. edited and revised manuscript; S.R.H., M.O.W., and H.-U.K. approved final version of manuscript.

REFERENCES

1. **Alford SK, van Beek EJ, McLennan G, Hoffman EA.** Heterogeneity of pulmonary perfusion as a mechanistic image-based phenotype in emphysema susceptible smokers. *Proc Natl Acad Sci USA* 107: 7485–7490, 2010.
2. **Almquist H, Jonson B, Palmer J, Valind S, Wollmer P.** Regional VA/Q ratios in man using 133Xe and single photon emission computed tomography (SPECT) corrected for attenuation. *Clin Physiol* 19: 475–481, 1999.
3. **Almquist HM, Palmer J, Jonson B, Wollmer P.** Pulmonary perfusion and density gradients in healthy volunteers. *J Nucl Med* 38: 962–966, 1997.
4. **Altemeier WA, McKinney S, Glenny RW.** Fractal nature of regional ventilation distribution. *J Appl Physiol* 88: 1551–1557, 2000.
5. **Amundsen T, Torheim G, Kvistad KA, Waage A, Bjermer L, Nordlid KK, Johnsen H, Asberg A, Haraldseth O.** Perfusion abnormalities in pulmonary embolism studied with perfusion MRI and ventilation-perfusion scintigraphy: an intra-modality and inter-modality agreement study. *J Magn Reson Imaging* 15: 386–394, 2002.
6. **Anderson DR, Kahn SR, Rodger MA, Kovacs MJ, Morris T, Hirsch A, Lang E, Stiell I, Kovacs G, Dreyer J, Dennie C, Cartier Y, Barnes D, Burton E, Pleasance S, Skedgel C, O'Rouke K, Wells PS.** Computed tomographic pulmonary angiography vs ventilation-perfusion lung scanning in patients with suspected pulmonary embolism: a randomized controlled trial. *JAMA* 298: 2743–2753, 2007.
7. **Anthonisen NR, Milic-Emili J** Distribution of pulmonary perfusion in erect man. *J Appl Physiol* 21: 760–766, 1966.
8. **Arai TJ, Henderson AC, Dubowitz DJ, Levin DL, Friedman PJ, Buxton RB, Prisk GK, Hopkins SR.** Hypoxic pulmonary vasoconstriction does not contribute to pulmonary blood flow heterogeneity in normoxia in normal supine humans. *J Appl Physiol* 106: 1057–1064, 2009.
9. **Arai TJ, Prisk GK, Holverda S, Sa RC, Theilmann RJ, Henderson AC, Cronin MV, Buxton RB, Hopkins SR.** Magnetic resonance imaging quantification of pulmonary perfusion using calibrated arterial spin labeling. *J Vis Exp* 30: 2712, 2011.
10. **Bankier AA, Tack D.** Dose reduction strategies for thoracic multidetector computed tomography: background, current issues, and recommendations. *J Thorac Imaging* 25: 278–288, 2010.
11. **Biederer J, Beer M, Hirsch W, Wild JM, Fabel M, Puderbach M, van Beek EJ.** MRI of the lung (2/3): Why . . . when how? *Insights Imaging*, 2011.
12. **Biederer J, Liess C, Charalambous N, Heller M.** Volumetric interpolated contrast-enhanced MRA for the diagnosis of pulmonary embolism in an ex vivo system. *J Magn Reson Imaging* 19: 428–437, 2004.
13. **Bolar DS, Levin DL, Hopkins SR, Frank LF, Liu TT, Wong EC, Buxton RB.** Quantification of regional pulmonary blood flow using ASL-FAIRER. *Magn Reson Med* 55: 1308–1317, 2006.
14. **Brimioulle S, Julien V, Gust R, Kozlowski JK, Naeije R, Schuster DP.** Importance of hypoxic vasoconstriction in maintaining oxygenation during acute lung injury. *Crit Care Med* 30: 874–880, 2002.

15. **Brudin LH, Rhodes CG, Valind SO, Jones T, Hughes JM.** Interrelationships between regional blood flow, blood volume, and ventilation in supine humans. *J Appl Physiol* 76: 1205–1210, 1994.
16. **Burrowes K, Buxton RB, Prisk GK.** Assessing potential errors of MRI-based measures of pulmonary blood flow using a detailed network flow model. *J Appl Physiol*; doi: 10.1152/japplphysiol.00894.2011.
17. **Buxton RB.** Quantifying CBF with arterial spin labeling. *J Magn Reson Imaging* 22: 723–726, 2005.
18. **Cao JJ, Wang Y, Schapiro W, McLaughlin J, Cheng J, Passick M, Ngai N, Marcus P, Reichek N.** Effects of respiratory cycle and body position on quantitative pulmonary perfusion by MRI. *J Magn Reson Imaging* 34: 225–230, 2011.
19. **Easley RB, Fuld MK, Fernandez-Bustamante A, Hoffman EA, Simon BA.** Mechanism of hypoxemia in acute lung injury evaluated by multidetector-row CT. *Acad Radiol* 13: 916–921, 2006.
20. **Eichinger M, Puderbach M, Fink C, Gahr J, Ley S, Plathow C, Tuengerthal S, Zuna I, Muller FM, Kauczor HU.** Contrast-enhanced 3D MRI of lung perfusion in children with cystic fibrosis—initial results. *Eur Radiol* 16: 2147–2152, 2006.
21. **Fan L, Liu SY, Xiao XS, Sun F.** Demonstration of pulmonary perfusion heterogeneity induced by gravity and lung inflation using arterial spin labeling. *Eur J Radiol* 73: 249–254, 2010.
22. **Fazel R, Krumholz HM, Wang Y, Ross JS, Chen J, Ting HH, Shah ND, Nasir K, Einstein AJ, Nallamothu BK.** Exposure to low-dose ionizing radiation from medical imaging procedures. *N Engl J Med* 361: 849–857, 2009.
23. **Fink C, Ley S, Kroeker R, Requardt M, Kauczor HU, Bock M.** Time-resolved contrast-enhanced three-dimensional magnetic resonance angiography of the chest: combination of parallel imaging with view sharing (TREAT). *Invest Radiol* 40: 40–48, 2005.
24. **Fink C, Ley S, Risse F, Eichinger M, Zaporozhan J, Buhmann R, Puderbach M, Plathow C, Kauczor HU.** Effect of inspiratory and expiratory breathhold on pulmonary perfusion: assessment by pulmonary perfusion magnetic resonance imaging. *Invest Radiol* 40: 72–79, 2005.
25. **Fink C, Ley S, Schoenberg SO, Reiser MF, Kauczor HU.** Magnetic resonance imaging of acute pulmonary embolism. *Eur Radiol* 17: 2546–2553, 2007.
26. **Fink C, Puderbach M, Bock M, Lodemann KP, Zuna I, Schmahl A, Delorme S, Kauczor HU.** Regional lung perfusion: assessment with partially parallel three-dimensional MR imaging. *Radiology* 231: 175–184, 2004.
27. **Gatehouse PD, Keegan J, Crowe LA, Masood S, Mohiaddin RH, Kreitner KF, Firmin DN.** Applications of phase-contrast flow and velocity imaging in cardiovascular MRI. *Eur Radiol* 15: 2172–2184, 2005.
28. **Glenny RW.** Heterogeneity in the lung: concepts and measures. In: *Complexity in Structure and Function in the Lung*, edited by Hlastala MP and Robertson HT. New York: Marcel Dekker, 1998, p. 571–609.
29. **Grosse-Wortmann L, Al-Otay A, Yoo SJ.** Aortopulmonary collaterals after bidirectional cavopulmonary connection or Fontan completion: quantification with MRI. *Circ Cardiovasc Imaging* 2: 219–225, 2009.
30. **Gustafsson A, Jacobsson L, Johansson A, Moonen M, Tylen U, Bake B.** Evaluation of various attenuation corrections in lung SPECT in healthy subjects. *Nucl Med Commun* 24: 1087–1095, 2003.
31. **Henderson AC, Levin DL, Hopkins SR, Olfert IM, Buxton RB, Prisk GK.** Steep head-down tilt has persisting effects on the distribution of pulmonary blood flow. *J Appl Physiol* 101: 583–589, 2006.
32. **Henderson AC, Levin DL, Hopkins SR, Olfert IM, Buxton RB, Prisk GK.** Steep head-down tilt has persisting effects on the distribution of pulmonary blood flow. *J Appl Physiol* 101: 583–589, 2006.
33. **Henderson AC, Prisk GK, Levin DL, Hopkins SR, Buxton RB.** Characterizing pulmonary blood flow distribution measured using arterial spin labeling. *NMR Biomed* 22: 1025–1035, 2009.
34. **Hoffman EA, Simon BA, McLennan G.** State of the art. A structural and functional assessment of the lung via multidetector-row computed tomography: phenotyping chronic obstructive pulmonary disease. *Proc Am Thorac Soc* 3: 519–532, 2006.
35. **Hopkins SR, Arai TJ, Henderson AC, Levin DL, Buxton RB, Kim Prisk G.** Lung volume does not alter the distribution of pulmonary perfusion in dependent lung in supine humans. *J Physiol* 588: 4759–4768, 2010.
36. **Hopkins SR, Garg J, Bolar D, Balouch J, Levin D.** Pulmonary blood flow heterogeneity during hypoxia in subjects with prior high altitude pulmonary edema (HAPE). *Am J Respir Crit Care Med* 171: 83–87, 2005.
37. **Hopkins SR, Garg J, Bolar DS, Balouch J, Levin DL.** Pulmonary blood flow heterogeneity during hypoxia and high-altitude pulmonary edema. *Am J Respir Crit Care Med* 171: 83–87, 2005.
38. **Hopkins SR, Henderson AC, Levin DL, Yamada K, Arai T, Buxton RB, Prisk GK.** Vertical gradients in regional lung density and perfusion in the supine human lung: the Slinky effect. *J Appl Physiol* 103: 240–248, 2007.
39. **Hopkins SR, Prisk GK.** Lung perfusion measured using magnetic resonance imaging: new tools for physiological insights into the pulmonary circulation. *J Magn Reson Imaging* 32: 1287–1301, 2010.
40. **Hsu LY, Groves DW, Aletras AH, Kellman P, Arai AE.** A quantitative pixel-wise measurement of myocardial blood flow by contrast-enhanced first-pass CMR perfusion imaging: microsphere validation in dogs and feasibility study in humans. *JACC Cardiovasc Imaging* 5: 154–166, 2012.
41. **Hughes JM, Glazier JB, Maloney JE, West JB.** Effect of lung volume on the distribution of pulmonary blood flow in man. *Respir Physiol* 4: 58–72, 1968.
42. **Johnson TR, Krauss B, Sedlmair M, Grasruck M, Bruder H, Morhard D, Fink C, Weckbach S, Lenhard M, Schmidt B, Flohr T, Reiser MF, Becker CR.** Material differentiation by dual energy CT: initial experience. *Eur Radiol* 17: 1510–1517, 2007.
43. **Kauczor HU, Cagil H, Fischer B, Schwickert HC, Mildenberger P.** [CT angiography of the bronchial arteries]. *Rofo Fortschr Geb Rontgenstr Neuen Bildgeb Verfahr* 160: 477–479, 1994.
44. **Kauczor HU, Wielpütz MO, Owsijewitsch M, Ley-Zaporozhan J.** Computed tomographic imaging of the airways in COPD and asthma. *J Thorac Imaging* 26: 290–300, 2011.
45. **Keilholz SD, Knight-Scott J, Christopher JM, Mai VM, Berr SS.** Gravity-dependent perfusion of the lung demonstrated with the FAIRER arterial spin tagging method. *Magn Reson Imaging* 19: 929–935, 2001.
46. **Kety S.** Measurement of local blood flow by the exchange of an inert, diffusible substance. *Methods Med Res* 8: 228–236, 1960.
47. **Kety SS.** The theory and applications of the exchange of inert gas at the lungs and tissues. *Pharmacol Rev* 3: 1–41, 1951.
48. **Ko JP, Brandman S, Stember J, Naidich DP.** Dual-energy computed tomography: concepts, performance, and thoracic applications. *J Thorac Imaging* 27: 7–22, 2012.
49. **Kosuda S, Kobayashi H, Kusano S.** Change in regional pulmonary perfusion as a result of posture and lung volume assessed using technetium-99m macroaggregated albumin SPET. *Eur J Nucl Med* 27: 529–535, 2000.
50. **Kubo T, Lin PJ, Stiller W, Takahashi M, Kauczor HU, Ohno Y, Hatabu H.** Radiation dose reduction in chest CT: a review. *AJR Am J Roentgenol* 190: 335–343, 2008.
51. **Kuriyama T, Latham LP, Horwitz LD, Reeves JT, Wagner WW Jr.** Role of collateral ventilation in ventilation-perfusion balance. *J Appl Physiol* 56: 1500–1506, 1984.
52. **Levin DL, Buxton RB, Spiess JP, Arai T, Balouch J, Hopkins SR.** Effects of age on pulmonary perfusion heterogeneity measured by magnetic resonance imaging. *J Appl Physiol* 102: 2064–2070, 2007.
53. **Ley S, Fink C, Puderbach M, Plathow C, Risse F, Kreitner KF, Kauczor HU.** [Contrast-enhanced 3D MR perfusion of the lung: application of parallel imaging technique in healthy subjects]. *Rofo Fortschr Geb Rontgenstr Neuen Bildgeb Verfahr* 176: 330–334, 2004.
54. **Ley S, Kauczor HU, Heussel CP, Kramm T, Mayer E, Thelen M, Kreitner KF.** Value of contrast-enhanced MR angiography and helical CT angiography in chronic thromboembolic pulmonary hypertension. *Eur Radiol* 13: 2365–2371, 2003.
55. **Ley S, Mereles D, Risse F, Grunig E, Ley-Zaporozhan J, Tecer Z, Puderbach M, Fink C, Kauczor HU.** Quantitative 3D pulmonary MR-perfusion in patients with pulmonary arterial hypertension: correlation with invasive pressure measurements. *Eur J Radiol* 61: 251–255, 2007.
56. **Ley S, Puderbach M, Fink C, Eichinger M, Plathow C, Teiner S, Wiebel M, Muller FM, Kauczor HU.** Assessment of hemodynamic changes in the systemic and pulmonary arterial circulation in patients with cystic fibrosis using phase-contrast MRI. *Eur Radiol* 15: 1575–1580, 2005.
57. **Ley-Zaporozhan J, Puderbach M, Kauczor HU.** MR for the evaluation of obstructive pulmonary disease. *Magn Reson Imaging Clin N Am* 16: 291–308, ix, 2008.

58. **Maeda H, Itoh H, Ishii Y, Todo G, Mukai T, Fujita M, Kambara H, Kawai C, Torizuka K.** Pulmonary blood flow distribution measured by radionuclide-computed tomography. *J Appl Physiol* 54: 225–233, 1983.
59. **Mai VM, Hagspeil KD, Christopher JM, Do HM, Altes T, Knight-Scott J, Stith AL, Maier T, Berr SS.** Perfusion imaging of the human lung using flow-sensitive alternating frequency inversion recovery with an extra radiofrequency pulse (FAIRER). *Magn Reson Med* 17: 355–361, 1999.
60. **Matsuoka S, Uchiyama K, Shima H, Terakoshi H, Oishi S, Nojiri Y, Ogata H.** Effect of the rate of gadolinium injection on magnetic resonance pulmonary perfusion imaging. *J Magn Reson Imaging* 15: 108–113, 2002.
61. **McCullagh A, Rosenthal M, Wanner A, Hurtado A, Padley S, Bush A.** The bronchial circulation—worth a closer look: a review of the relationship between the bronchial vasculature and airway inflammation. *Pediatr Pulmonol* 45: 1–13, 2009.
62. **Mettler FA Jr, Huda W, Yoshizumi TT, Mahesh M.** Effective doses in radiology and diagnostic nuclear medicine: a catalog. *Radiology* 248: 254–263, 2008.
63. **Mintun MA, Ter-Pogossian MM, Green MA, Lich LL, Schuster DP.** Quantitative measurement of regional pulmonary blood flow with positron emission tomography. *J Appl Physiol* 60: 317–326, 1986.
64. **Morino S, Toba T, Araki M, Azuma T, Tsutsumi S, Tao H, Nakamura T, Nagayasu T, Tagawa T.** Noninvasive assessment of pulmonary emphysema using dynamic contrast-enhanced magnetic resonance imaging. *Exp Lung Res* 32: 55–67, 2006.
65. **Musch G, Layfield JD, Harris RS, Melo MF, Winkler T, Callahan RJ, Fischman AJ, Venegas JG.** Topographical distribution of pulmonary perfusion and ventilation, assessed by PET in supine and prone humans. *J Appl Physiol* 93: 1841–1851, 2002.
66. **Musch G, Venegas JG.** Positron emission tomography imaging of regional lung function. *Minerva Anestesiol* 72: 363–367, 2006.
67. **Musch G, Venegas JG.** Positron emission tomography imaging of regional pulmonary perfusion and ventilation. *Proc Am Thorac Soc* 2: 508–529, 2005.
68. **Nakazawa T, Watanabe Y, Hori Y, Kiso K, Higashi M, Itoh T, Naito H.** Lung perfused blood volume images with dual-energy computed tomography for chronic thromboembolic pulmonary hypertension: correlation to scintigraphy with single-photon emission computed tomography. *J Comput Assist Tomogr* 35: 590–595, 2011.
69. **Neeb D, Kunz RP, Ley S, Szabo G, Strauss LG, Kauczor HU, Kreitner KF, Schreiber LM.** Quantification of pulmonary blood flow (PBF): validation of perfusion MRI and nonlinear contrast agent (CA) dose correction with H(2)15O positron emission tomography (PET). *Magn Reson Med* 62: 476–487, 2009.
70. **Ohno Y, Hatabu H, Murase K, Higashino T, Kawamitsu H, Watanabe H, Takenaka D, Fujii M, Sugimura K.** Quantitative assessment of regional pulmonary perfusion in the entire lung using three-dimensional ultrafast dynamic contrast-enhanced magnetic resonance imaging: preliminary experience in 40 subjects. *J Magn Reson Imaging* 20: 353–365, 2004.
71. **Orphanidou D, Hughes JM, Myers MJ, Al-Suhali AR, Henderson B.** Tomography of regional ventilation and perfusion using krypton 81m in normal subjects and asthmatic patients. *Thorax* 41: 542–551, 1986.
72. **Petersen SE, Voigtlander T, Kreitner KF, Kalden P, Wittlinger T, Scharhag J, Horstick G, Becker D, Hommel G, Thelen M, Meyer J.** Quantification of shunt volumes in congenital heart diseases using a breath-hold MR phase contrast technique–comparison with oximetry. *Int J Cardiovasc Imaging* 18: 53–60, 2002.
73. **Petersson J, Ax M, Frey J, Sanchez-Crespo A, Lindahl SG, Mure M.** Positive end-expiratory pressure redistributes regional blood flow and ventilation differently in supine and prone humans. *Anesthesiology* 113: 1361–1369, 2010.
74. **Petersson J, Rohdin M, Sanchez-Crespo A, Nyren S, Jacobsson H, Larsson SA, Lindahl SG, Linnarsson D, Glenny RW, Mure M.** Paradoxical redistribution of pulmonary blood flow in prone and supine humans exposed to hypergravity. *J Appl Physiol* 100: 240–248, 2006.
75. **Petersson J, Rohdin M, Sanchez-Crespo A, Nyren S, Jacobsson H, Larsson SA, Lindahl SG, Linnarsson D, Neradilek B, Polissar NL, Glenny RW, Mure M.** Posture primarily affects lung tissue distribution with minor effect on blood flow and ventilation. *Respir Physiol Neurobiol* 156: 293–303, 2007.
76. **Petersson J, Rohdin M, Sanchez-Crespo A, Nyren S, Jacobsson H, Larsson SA, Lindahl SG, Linnarsson D, Neradilek B, Polissar NL, Glenny RW, Mure M.** Regional lung blood flow and ventilation in upright humans studied with quantitative SPECT. *Respir Physiol Neurobiol* 166: 54–60, 2009.
77. **Petersson J, Sanchez-Crespo A, Larsson SA, Mure M.** Physiological imaging of the lung: single-photon-emission computed tomography (SPECT). *J Appl Physiol* 102: 468–476, 2007.
78. **Petersson J, Sanchez-Crespo A, Rohdin M, Montmerle S, Nyren S, Jacobsson H, Larsson SA, Lindahl SG, Linnarsson D, Glenny RW, Mure M.** Physiological evaluation of a new quantitative SPECT method measuring regional ventilation and perfusion. *J Appl Physiol* 96: 1127–1136, 2004.
79. **Pontana F, Faivre JB, Remy-Jardin M, Flohr T, Schmidt B, Tacelli N, Pansini V, Remy J.** Lung perfusion with dual-energy multidetector-row CT (MDCT): feasibility for the evaluation of acute pulmonary embolism in 117 consecutive patients. *Acad Radiol* 15: 1494–1504, 2008.
80. **Prisk GK, Yamada K, Henderson AC, Arai TJ, Levin DL, Buxton RB, Hopkins SR.** Pulmonary perfusion in the prone and supine postures in the normal human lung. *J Appl Physiol* 103: 883–894, 2007.
81. **Prisk GK, Yamada K, Henderson AC, Arai TJ, Levin DL, Buxton RB, Hopkins SR.** Pulmonary perfusion in the prone and supine postures in the normal human lung. *J Appl Physiol* 103: 883–894, 2007.
82. **Puderbach M, Hintze C, Ley S, Eichinger M, Kauczor HU, Biederer J.** MR imaging of the chest: a practical approach at 1.5T. *Eur J Radiol* 64: 345–355, 2007.
83. **Puderbach M, Risse F, Biederer J, Ley-Zaporozhan J, Ley S, Szabo G, Semmler W, Kauczor HU.** In vivo Gd-DTPA concentration for MR lung perfusion measurements: assessment with computed tomography in a porcine model. *Eur Radiol* 18: 2102–2107, 2008.
84. **Rhodes CG, Hughes JM.** Pulmonary studies using positron emission tomography. *Eur Respir J* 8: 1001–1017, 1995.
85. **Rossi A, Attina D, Borgonovi A, Buia F, De Luca F, Guidalotti PL, Fughelli P, Galie N, Zompatori M.** Evaluation of mosaic pattern areas in HRCT with Min-IP reconstructions in patients with pulmonary hypertension: Could this evaluation replace lung perfusion scintigraphy? *Eur J Radiol* 81: e1–e6, 2012.
86. **Sanchez-Crespo A, Petersson J, Nyren S, Mure M, Glenny RW, Thorell JO, Jacobsson H, Lindahl SG, Larsson SA.** A novel quantitative dual-isotope method for simultaneous ventilation and perfusion lung SPET. *Eur J Nucl Med* 29: 863–875, 2002.
87. **Sasse SA, Berry RB, Nguyen TK, Light RW, Mahutte CK.** Arterial blood gas changes during breath-holding from functional residual capacity. *Chest* 110: 958–964, 1996.
88. **Schuster DP, Anderson C, Kozlowski J, Lange N.** Regional pulmonary perfusion in patients with acute pulmonary edema. *J Nucl Med* 43: 863–870, 2002.
89. **Schuster DP, Kaplan JD, Gauvain K, Welch MJ, Markham J.** Measurement of regional pulmonary blood flow with PET. *J Nucl Med* 36: 371–377, 1995.
90. **Suzuki H, Sato Y, Shindo M, Yoshioka H, Mizutani T, Onizuka M, Sakakibara Y.** Prone positioning improves distribution of pulmonary perfusion: noninvasive magnetic resonance imaging study in healthy humans. *Eur Radiol* 18: 522–528, 2008.
91. **Swenson ER, Domino KB, Hlastala MP.** Physiological effects of oxygen and carbon dioxide on VA/Q heterogeneity. In: *Complexity in Structure and Function in the Lung*, edited by Hlastala MP and Robertson HT. New York: Marcel Dekker, 1998, p. 511–547.
92. **Thabut G, Dauriat G, Stern JB, Logeart D, Levy A, Marrash-Chahla R, Mal H.** Pulmonary hemodynamics in advanced COPD candidates for lung volume reduction surgery or lung transplantation. *Chest* 127: 1531–1536, 2005.
93. **Thieme SF, Becker CR, Hacker M, Nikolaou K, Reiser MF, Johnson TR.** Dual energy CT for the assessment of lung perfusion—correlation to scintigraphy. *Eur J Radiol* 68: 369–374, 2008.
94. **Thieme SF, Graute V, Nikolaou K, Maxien D, Reiser MF, Hacker M, Johnson TR.** Dual energy CT lung perfusion imaging—correlation with SPECT/CT. *Eur J Radiol* 81: 360–365, 2012.
96. **Thieme SF, Johnson TR, Lee C, McWilliams J, Becker CR, Reiser MF, Nikolaou K.** Dual-energy CT for the assessment of contrast material distribution in the pulmonary parenchyma. *AJR Am J Roentgenol* 193: 144–149, 2009.
97. **Uematsu H, Levin DL, Hatabu H.** Quantification of pulmonary perfusion with MR imaging: recent advances. *Eur J Radiol* 37: 155–163, 2001.
98. **Valverde I, Rachel C, Kuehne T, Beerbaum P.** Comprehensive four-dimensional phase-contrast flow assessment in hemi-Fontan circulation:

systemic-to-pulmonary collateral flow quantification. *Cardiol Young* 21: 116–119, 2011.

99. **van Amerom JF, Vidarsson L, Wu S, Tessler R, Yoo SJ, Belik J, Macgowan CK.** Regional pulmonary blood flow: Comparison of dynamic contrast-enhanced MR perfusion and phase-contrast MR. *Magn Reson Med* 61: 1249–1254, 2009.
100. **Vidal Melo MF, Layfield D, Harris RS, O'Neill K, Musch G, Richter T, Winkler T, Fischman AJ, Venegas JG.** Quantification of regional ventilation-perfusion ratios with PET. *J Nucl Med* 44: 1982–1991, 2003.
101. **Vidal Melo MF, Winkler T, Harris RS, Musch G, Greene RE, Venegas JG.** Spatial heterogeneity of lung perfusion assessed with (13)N PET as a vascular biomarker in chronic obstructive pulmonary disease. *J Nucl Med* 51: 57–65, 2010.
102. **West JB, Dollery CT, Hugh-Jones P.** The use of radioactive carbon dioxide to measure regional blood flow in the lungs of patients with pulmonary disease. *J Clin Invest* 40: 1–12, 1961.
103. **West JB, Dollery CT, Naimark A.** Distribution of blood flow in isolated lung; Relation to vascular and alveolar pressures. *J Appl Physiol* 19: 713–724, 1964.
104. **Won C, Chon D, Tajik J, Tran BQ, Robinswood GB, Beck KC, Hoffman EA.** CT-based assessment of regional pulmonary microvascular blood flow parameters. *J Appl Physiol* 94: 2483–2493, 2003.
105. **Wook Lee C, Beom Seo J, Lee Y, Jin Chae E, Kim N, Joo Lee H, Jeon Hwang H, Lim CH.** A pilot trial on pulmonary emphysema quantification and perfusion mapping in a single-step using contrast-enhanced dual-energy computed tomography. *Invest Radiol* 47: 92–97, 2012.